



TECHNICAL REPORT

Smart Body Area Networks (SmartBAN); Implant communications

Reference

DTR/SmartBAN-003

Keywords

health, implants, protocol

ETSI

650 Route des Lucioles
F-06921 Sophia Antipolis Cedex - FRANCE

Tel.: +33 4 92 94 42 00 Fax: +33 4 93 65 47 16

Siret N° 348 623 562 00017 - APE 7112B
Association à but non lucratif enregistrée à la
Sous-Préfecture de Grasse (06) N° w061004871

Important notice

The present document can be downloaded from:

<http://www.etsi.org/standards-search>

The present document may be made available in electronic versions and/or in print. The content of any electronic and/or print versions of the present document shall not be modified without the prior written authorization of ETSI. In case of any existing or perceived difference in contents between such versions and/or in print, the prevailing version of an ETSI deliverable is the one made publicly available in PDF format at www.etsi.org/deliver.

Users of the present document should be aware that the document may be subject to revision or change of status.

Information on the current status of this and other ETSI documents is available at

<https://portal.etsi.org/TB/ETSIDeliverableStatus.aspx>

If you find errors in the present document, please send your comment to one of the following services:

<https://portal.etsi.org/People/CommitteeSupportStaff.aspx>

Notice of disclaimer & limitation of liability

The information provided in the present deliverable is directed solely to professionals who have the appropriate degree of experience to understand and interpret its content in accordance with generally accepted engineering or other professional standard and applicable regulations.

No recommendation as to products and services or vendors is made or should be implied.

No representation or warranty is made that this deliverable is technically accurate or sufficient or conforms to any law and/or governmental rule and/or regulation and further, no representation or warranty is made of merchantability or fitness for any particular purpose or against infringement of intellectual property rights.

In no event shall ETSI be held liable for loss of profits or any other incidental or consequential damages.

Any software contained in this deliverable is provided "AS IS" with no warranties, express or implied, including but not limited to, the warranties of merchantability, fitness for a particular purpose and non-infringement of intellectual property rights and ETSI shall not be held liable in any event for any damages whatsoever (including, without limitation, damages for loss of profits, business interruption, loss of information, or any other pecuniary loss) arising out of or related to the use of or inability to use the software.

Copyright Notification

No part may be reproduced or utilized in any form or by any means, electronic or mechanical, including photocopying and microfilm except as authorized by written permission of ETSI.

The content of the PDF version shall not be modified without the written authorization of ETSI.

The copyright and the foregoing restriction extend to reproduction in all media.

© ETSI 2021.

All rights reserved.

Contents

Intellectual Property Rights	6
Foreword.....	6
Modal verbs terminology.....	6
1 Scope	7
2 References	7
2.1 Normative references	7
2.2 Informative references.....	7
3 Definition of terms, symbols and abbreviations.....	7
3.1 Terms.....	7
3.2 Symbols.....	7
3.3 Abbreviations	7
4 Introduction and Background.....	8
5 Implant UWB Communication System.....	9
5.1 Transmitter structure	9
5.2 Receiver structure.....	9
6 Fundamental Performance Evaluation	10
6.1 Setup.....	10
6.2 Results and Discussions	11
7 Evaluation with Living Animal Experiment	11
7.1 Setup.....	11
7.2 Results and Discussions	12
8 MIMO Transmission for Implant UWB-IR System.....	13
8.1 Antenna Development for Implant Side Polarization Diversity.....	13
8.2 Experimental Evaluation on Path Loss Characteristics	13
8.3 Improvement of communication performance	14
9 Implantable Device Localization with UWB Communications	15
9.1 Location Estimation System Based on RSSI.....	15
9.2 Experimental Evaluation on RSSI-Based Localization	16
9.3 Location Estimation System Based on TOA	17
9.4 Performance Evaluation on TOA-Based Localization	18
History	20

List of figures

Figure 1: Implant UWB-IR system structure	9
Figure 2: An example of UWB-IR modulated signals	9
Figure 3: Examples of shapes of transmitted and received signals	10
Figure 4: Path loss characteristics of liquid phantom.....	10
Figure 5: BER performance evaluation in liquid phantom experiment.....	11
Figure 6: Overview of living animal experiment	12
Figure 7: BER performance evaluation in living animal experiment.....	12
Figure 8: Developed diversity antenna for implant UWB communication (a) Planar elliptical loop antenna (b) Bird's-eye view of the dual-polarized diversity antenna.....	13
Figure 9: Overview of experimental environment with a living animal.....	14
Figure 10: Measured path loss performance in the experiment.....	14
Figure 11: Cumulative distribution function of SNR characteristics.....	15
Figure 12: Location estimation system.....	16
Figure 13: Experimental setup for RSSI-based localization system.....	16
Figure 14: Cumulative distribution function on position estimation error	17
Figure 15: Validation results for relative permittivity estimation model	18
Figure 16: RMSE location estimation error for TOA-based location estimation method	19
Figure 17: <i>c.d.f.</i> of location estimation error for TOA-based localization	19

List of tables

Table 1: Parameters of communication performance evaluation	14
---	----

Intellectual Property Rights

Essential patents

IPRs essential or potentially essential to normative deliverables may have been declared to ETSI. The declarations pertaining to these essential IPRs, if any, are publicly available for **ETSI members and non-members**, and can be found in ETSI SR 000 314: "*Intellectual Property Rights (IPRs); Essential, or potentially Essential, IPRs notified to ETSI in respect of ETSI standards*", which is available from the ETSI Secretariat. Latest updates are available on the ETSI Web server (<https://ipr.etsi.org/>).

Pursuant to the ETSI Directives including the ETSI IPR Policy, no investigation regarding the essentiality of IPRs, including IPR searches, has been carried out by ETSI. No guarantee can be given as to the existence of other IPRs not referenced in ETSI SR 000 314 (or the updates on the ETSI Web server) which are, or may be, or may become, essential to the present document.

Trademarks

The present document may include trademarks and/or tradenames which are asserted and/or registered by their owners. ETSI claims no ownership of these except for any which are indicated as being the property of ETSI, and conveys no right to use or reproduce any trademark and/or tradename. Mention of those trademarks in the present document does not constitute an endorsement by ETSI of products, services or organizations associated with those trademarks.

DECT™, **PLUGTESTS™**, **UMTS™** and the ETSI logo are trademarks of ETSI registered for the benefit of its Members. **3GPP™** and **LTE™** are trademarks of ETSI registered for the benefit of its Members and of the 3GPP Organizational Partners. **oneM2M™** logo is a trademark of ETSI registered for the benefit of its Members and of the oneM2M Partners. **GSM®** and the GSM logo are trademarks registered and owned by the GSM Association.

Foreword

This Technical Report (TR) has been produced by ETSI Technical Committee Smart Body Area Network (SmartBAN).

Modal verbs terminology

In the present document "**should**", "**should not**", "**may**", "**need not**", "**will**", "**will not**", "**can**" and "**cannot**" are to be interpreted as described in clause 3.2 of the [ETSI Drafting Rules](#) (Verbal forms for the expression of provisions).

"**must**" and "**must not**" are **NOT** allowed in ETSI deliverables except when used in direct citation.

1 Scope

The present document has the scope to evaluate ultra-low power, Ultra-WideBand technology (UWB) for a swallowable, pill-camera, wireless medical device operating in the 3,1 GHz to 10,6 GHz frequency band within the context of Smart Body Area Networks (SmartBAN).

2 References

2.1 Normative references

Normative references are not applicable in the present document.

2.2 Informative references

References are either specific (identified by date of publication and/or edition number or version number) or non-specific. For specific references, only the cited version applies. For non-specific references, the latest version of the reference document (including any amendments) applies.

NOTE: While any hyperlinks included in this clause were valid at the time of publication, ETSI cannot guarantee their long term validity.

The following referenced documents are not necessary for the application of the present document but they assist the user with regard to a particular subject area.

Not applicable.

3 Definition of terms, symbols and abbreviations

3.1 Terms

Void.

3.2 Symbols

Void.

3.3 Abbreviations

For the purposes of the present document, the following abbreviations apply:

ADC	Analog-to-Digital Converter
BAN	Body Area Network
BER	Bit Error Rate
BPF	Band Pass Filter
BPSK	Binary Phase Shift Keying
CMOS	Complementary Metal Oxide Semiconductor
CT	Computed Tomography
FDTD	Finite-Difference Time-Domain
FPGA	Field Programmable Gate Array
FSK	Frequency Shift Keying
IR	Impulse Radio
MICS	Medical Implant Communication Service
MIMO	Multiple-Input Multiple Output

ML	Maximum Likelihood
MPPM	Multi Position Pulse Modulation
MRC	Maximum Ratio Combining
MRI	Magnetic Resonance Imaging
OFDM	Orthogonal Frequency Division Multiplexing
RF	Radio Frequency
RMS	Root Mean Square
RMSE	Root Mean Square Error
RSSI	Received Signal Strength Indicator
SNR	Signal-to-Noise power Ratio
TOA	Time Of Arrival
UWB	Ultra WideBand
WCE	Wireless Capsule Endoscope

4 Introduction and Background

BANs attracted a lot of attention as a future technology for wireless networks. Typical applications of wireless BANs include healthcare, medical treatment and medical monitoring. Generally, wireless BANs are classified into two groups: wearable BANs and implant BANs. Wearable BANs are mainly used to monitor a person's healthy condition in daily life, whereas Wireless Capsule Endoscopy (WCE) has been one of the most important applications in implant BANs. WCE involves swallowing a small capsule by a patient, which contains a colour camera, light source, battery and transmits images to the outside receiver in order to assist in diagnosing gastrointestinal conditions such as obscure malabsorption, gastrointestinal bleeding, chronic diarrhoea and abdominal pain. The present document focuses on implant BAN applications. Such a medical application requires a reliable wireless communication channel and extremely low power consumption for increasing device longevity.

To realize the implant communications, the 400 MHz band and 2,4 GHz band are usually chosen. For example, a commercially available implant communication chip for cardiac pacemaker employs the 400 MHz band for data transmission and the 2,4 GHz band for waking-up and control. It has been reported that all of WCE techniques employ 400 MHz, 2,4 GHz or dozens of MHz band with narrow-band modulation schemes, such as Frequency Shift Keying (FSK) or Binary Phase Shift Keying (BPSK). The data rate is limited to several hundred kbps. However, in view of the implant communication application, for instance, WCE requires a higher data rate for a real-time image and video transmission.

In order to satisfy the above requirements, the present document pays attention to Ultra-Wideband (UWB) transmission. As UWB transmission schemes, UWB-Impulse Radio (UWB-IR), direct sequence-UWB (DS-UWB), and multiband-Orthogonal Frequency Division Multiplexing (multiband-OFDM) have been considered so far. Of all UWB schemes, UWB-IR is a technique that iteratively transmits extremely short pulses on the nanosecond time duration per bit. Therefore, it has merit in respect of low power consumption. Furthermore, coherent detection, namely correlation detection, claims to be one of the most suitable solutions for the UWB-IR communication system. Although the coherent detection needs to generate a template signal in the receiver side, the reliability of the coherent detection is generally superior to that of a non-coherent detection.

In implant BANs, the UWB-IR signals suffer from large attenuation, which may lead to undesired performance degradation. Therefore, it is important to investigate the transmission performance of the implant BANs. The present document aims to analyse the basic characteristics of the UWB-IR communication system by a liquid phantom experiment and then, evaluate the realistic performance of the implant UWB-IR system in a living animal experiment. In addition, Multiple-Input Multiple-Output (MIMO) technology is then considered for further improving the implant UWB communications. For this purpose, an example of implant side diversity antenna is developed, and the fundamental performance of the developed implant antenna is experimentally evaluated. Based on the measurement results, the communication performance improvement is discussed.

In the present document, the location estimation of an implantable device in UWB communications is also discussed. In medical treatments with implantable devices, it is important to estimate their locations accurately. So far, several kinds of localization methods have been proposed, such as magnetic field-based, Radio Frequency (RF) wave-based, and acoustic-based technologies. The present document pays attention to the Received Signal Strength Indicator (RSSI)-based localization because RSSI can be measured by a fundamental function in modern wireless communication systems without any additional special devices. High distance resolution of UWB (Ultra Wideband) communication signals is expected to achieve, as compared with a typical 400 MHz MICS band. In addition, this paper introduces an example of implant device localization systems based on UWB communications, and then discuss the achievable location estimation accuracy in a real environment.

5 Implant UWB Communication System

5.1 Transmitter structure

The structure of the transmitter is shown in Figure 1(a). As a UWB-IR pulse, the first order Gaussian monocycle pulse is employed, and this transmitter uses a Multi-Pulse Position Modulation (MPPM) scheme, which can control the trade-off relationship between the data rate and the reliability of the transmission. Figure 2 shows an example of MPPM signals when the number of chip slots L is set to 4, in which two UWB-IR pulses are assigned to each transmitted symbol. It is possible to control the data rate by changing the number of chip slots L . It is noted that the IR-type transmitter does not need a carrier signal and amplifiers. It employs a clock generator and some CMOS gates to produce pulses and a Band Pass Filter (BPF) for spectrum forming. Since CMOS gates consume low power and the passive BPF does not consume power, the total power consumption in the transmitter can be expected at a quite low level.

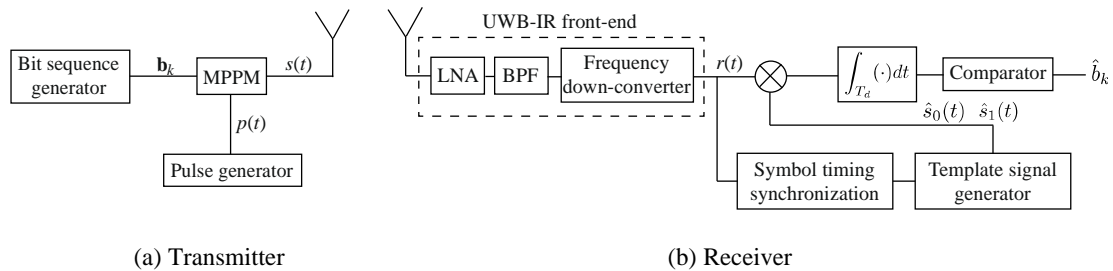


Figure 1: Implant UWB-IR system structure

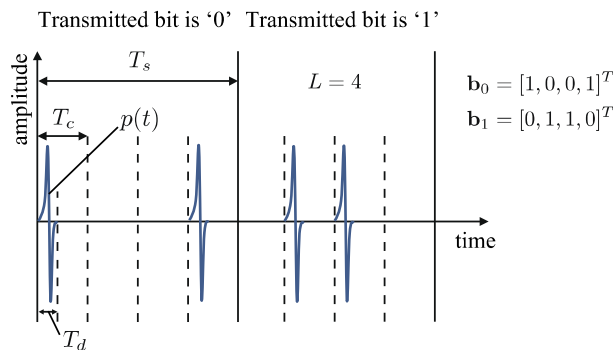


Figure 2: An example of UWB-IR modulated signals

5.2 Receiver structure

Figure 1(b) shows the structure of the receiver. From pre-measurement of the implant channel characteristics, it is found that the power delay profile can be well represented as a two-path model with a very small mean time interval in the order of nanoseconds. This means that the multipaths are almost indistinguishable in the received signal and the multipath fading effect is not dominative. Therefore a detection system without any channel estimation is suitable for the implant communications, so the correlation detection is herein considered as the receive detection scheme. In the correlation detection, since the binary MPPM chooses one from two location assignments, two kinds of energies for the corresponding pulse locations from the received signal are calculated. It is noted that the receiver requires no threshold for the detection. In Figure 1(b), the symbol timing synchronization is realized with pilot signals sent from the transmitter.

6 Fundamental Performance Evaluation

6.1 Setup

This clause demonstrates the fundamental performance of the implant UWB-IR communication system. For this purpose, the fundamental characteristics are experimentally measured in a liquid phantom environment simulating a human body. In this experiment, the helical antenna as an on-body receive antenna is used on the liquid phantom surface with a spacing of 1 cm. The in-body transmit antenna is a one-wavelength loop antenna. A type of glue is coated to the antenna and feeding part for preventing a direct contact of the antenna to the liquid. The transmit antenna was inserted in the liquid phantom. The liquid phantom was produced to simulate muscle-like dielectric properties. It is confirmed that the dielectric properties of the vessel and found that its loss is almost ignorable. The transmit and receive antennas are connected to a network analyser with coaxial cables. The two coaxial cables were arranged at a right angle each other for removing possible direct coupling between them. Figure 3 shows examples of shapes of the transmitted and received UWB signals. The S_{21} performance is measured, namely the path loss characteristic, as a function of the distance from the implant transmit antenna to the phantom surface at the frequency band of 4 GHz. The measured path loss characteristics are shown in Figure 4. It is found that at a depth of 70 mm from the body surface, the path loss is around 80 dB. Such a path loss level may be acceptable in present transceiver design technology.

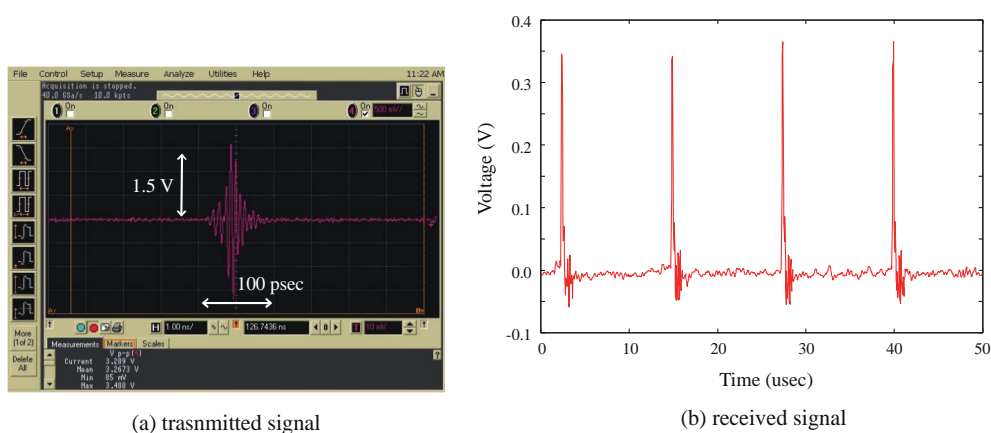


Figure 3: Examples of shapes of transmitted and received signals

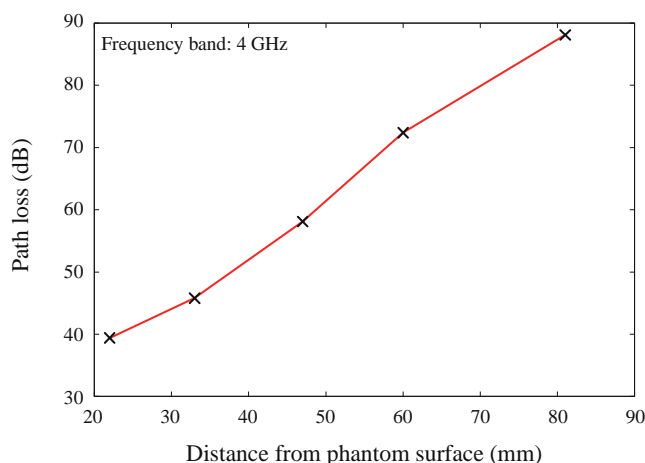


Figure 4: Path loss characteristics of liquid phantom

6.2 Results and Discussions

The BER performance of the UWB-IR transceivers is calculated based on the path loss measurement results in the liquid phantom experiment. It is assumed that the transmitter and the receiver were connected with an attenuator in order to accurately control the path loss according to the distance between transceivers, and then the BER is calculated from the comparison between the transmitted bit sequence and the received bit sequence. As for the symbol timing and sampling clock synchronization, it is almost perfectly performed with a proper length of pilot signals in the experiment. Moreover, the optimal detection time is also determined before conducting the experiment.

Figure 5 illustrates the average BER performances by the experiment and the theoretical analysis against the distance between transceivers. Good agreements are observed between the results of the experiment and the theory. Furthermore, as seen from Figure 5, the BER performance is improved as the data rate decreases (namely, L increases). Note that the BER performance of 10^{-2} is accomplished at the distance of around 70 mm when $L = 16$ (namely, the data rate is 1 Mbps). The achievement of the BER performance of around 10^{-2} to 10^{-3} means that it is possible to obtain an error-free BER ($< 10^{-10}$) if an adequate forward error correction code is adopted. This error-free BER satisfies the requirement for almost all implant BAN applications. Therefore, the developed UWB-IR communication system can establish a reliable communication link at the maximum distance of 70 mm in the biological-equivalent liquid phantom.

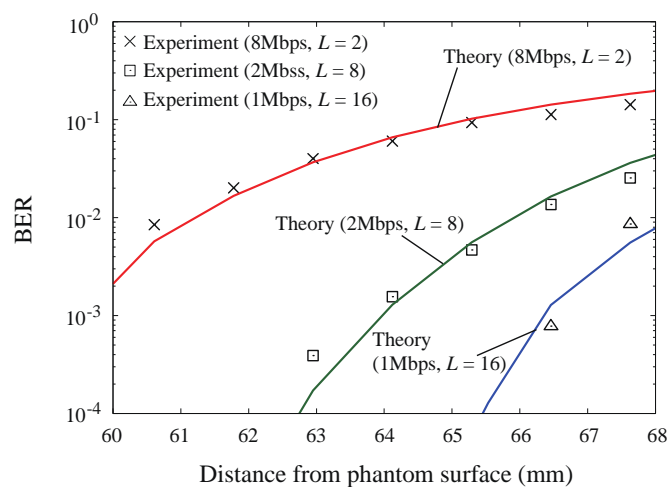


Figure 5: BER performance evaluation in liquid phantom experiment

7 Evaluation with Living Animal Experiment

7.1 Setup

Figure 6 shows an overview of the living body experiment with the developed UWB-IR system. In the living body experiment, a living animal (pig) is used instead of a human body because it is difficult to conduct an experiment with a living human body in our environment. The transmit antenna is implanted into the pig, and the receive antenna is put on the pig-body's surface. The transceivers and each antenna are connected with coaxial cables. For the received data capture, a laptop computer is connected to the receiver. The insertion points of the transmit antenna and the positions of the transmit antennas are shown in Figure 6, which indicates the transmit antenna positions when the insertion point is in the centre of the abdomen and the thorax (chest). In the experiment, the transmit antenna is covered with a vinyl material for insulation. The receive antenna is just above the transmit antenna on the body surface.

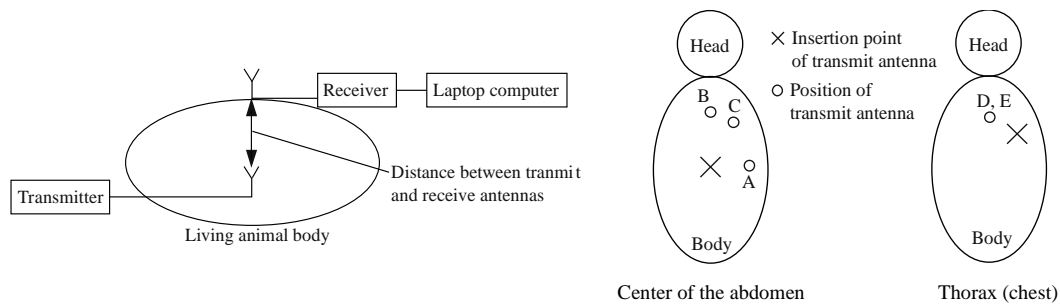


Figure 6: Overview of living animal experiment

7.2 Results and Discussions

Figure 7 illustrates the BER performance against the distance between transmit and receive antennas in the case of the Vivaldi-type receive antenna and the helical-type receive antenna. In this figure, the antenna position IDs are also indicated. Note that, in both antenna cases, no bit error is observed at the distance of 22 mm (Position ID: A), and moreover, in the helical antenna case, no bit error is observed also at the distance of 33 mm (Position ID: D). As for the reason that there is a sharp drop after 10^{-3} at 2 Mbps and 1 Mbps, it is because that the transmitted data number is not sufficient for giving an average BER in this order. Similarly to the result of the fundamental characteristic investigation in the previous clause, the evaluation results illustrate that the BER performances are inversely proportional to the data rate. Furthermore, as the distance between the antennas increases, the BER performance is getting worse due to the corresponding path loss in the biological tissues.

However, the BER at a distance of 80 mm exhibited a worse performance compared to that at 120 mm, which means that the BER performances are not always getting worse when the communication distance increases. This is because of the difference in the types and thickness of the tissue between the transceivers. A high-water-content tissue such as muscle and peritoneal fluid has a larger path loss, whereas a low-water-content tissue such as fat and bone has a smaller path loss. The implant communication performance is therefore dependent on not only the distance but also the types and thickness of the tissue between the transceivers, which explains why the results for the antennas placed in the five positions exhibit such distance dependence. Therefore, the transmission path is influenced by different tissue types which possess different dielectric properties. Therefore, it is necessary to consider not only the distance between the transceivers but also the penetrated tissues. To specify the effect of the penetrated tissues in detail, more investigation is required. In total, the developed UWB-IR communication system can achieve the BER performance of around 10^{-2} at the data rate of 1 Mbps up to a distance of 120 mm.

As compared between the results in the case of the Vivaldi antenna and the helical antenna, the BER performance of the helical antenna is better than that of the Vivaldi antenna. The difference in the BER performance may be attributed to the beam patterns of antennas and the polarization mismatch. Half power beam width of the circular polarized helical antenna is smaller than the beam width of the linear polarized Vivaldi antenna. This results in a higher gain and a lower polarization dependency of the signal received by the helical antenna.

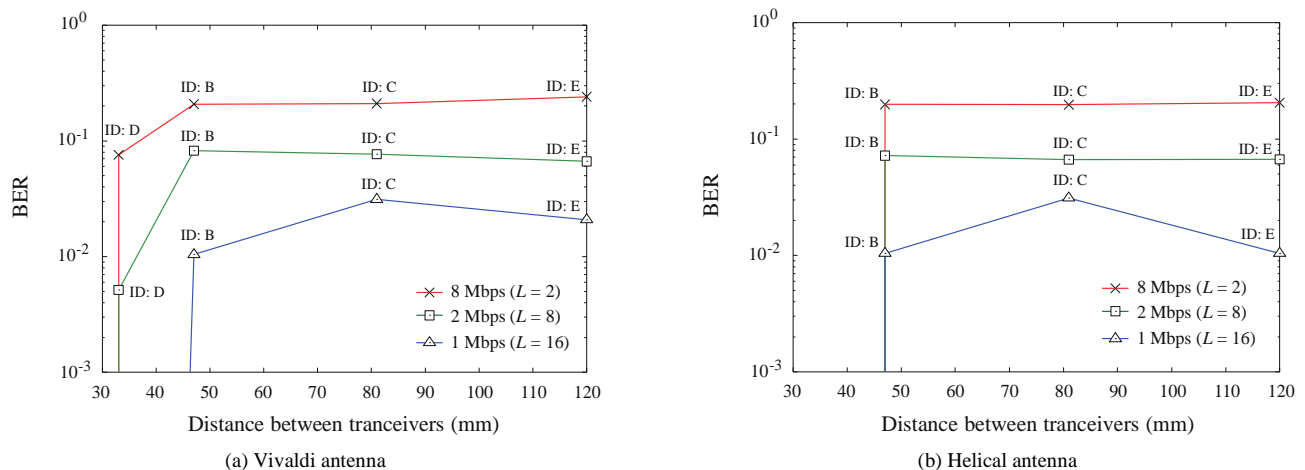


Figure 7: BER performance evaluation in living animal experiment

8 MIMO Transmission for Implant UWB-IR System

8.1 Antenna Development for Implant Side Polarization Diversity

This paper assumes a polarization diversity at an implant transmitter as a diversity technique. In order to accomplish the polarization diversity at the implant transmitter, two planar loop antennas were combined to develop an implant-side diversity antenna. Additionally, a low reflection coefficient and low coupling effect between each antenna element are required to realize the polarization diversity in the UWB low band. The design of one antenna element of dual-polarized diversity antenna in Figure 8 (a), where a dielectric substrate with a thickness of 1,6 mm and a relative permittivity of 4,0 is used. Also, Figure 8 (b) demonstrates the bird's-eye view of the dual-polarized implant antenna. For the elliptical loop shown in Figure 8 (a), the major and minor axes were set to 4,8 mm and 3,4 mm, respectively. The copper with a thickness of 0,1 mm was used for the loop antenna. It can be seen from Figure 8 (b) that one loop is arranged along a horizontal direction (on x-y plane) and the other one is arranged along a vertical direction (on y-z plane) without touching each other.

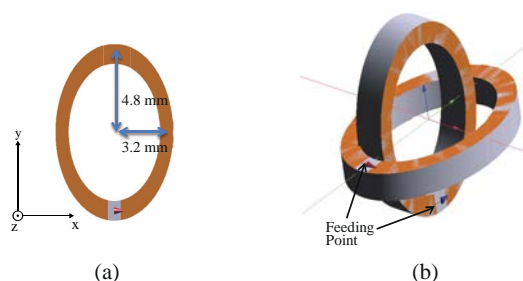


Figure 8: Developed diversity antenna for implant UWB communication
(a) Planar elliptical loop antenna
(b) Bird's-eye view of the dual-polarized diversity antenna

8.2 Experimental Evaluation on Path Loss Characteristics

The developed diversity antenna was evaluated in a living animal experiment in terms of fundamental performance including the path loss characteristics. The environment of the living animal environment is shown in Figure 9. As shown in the cross-sectional overview of the living animal experiment in Figure 9, the developed diversity antenna was implanted into the animal body, and the receive antenna was put on the surface of the body. Laparotomy surgery was done to allow implantation of the implant side diversity antenna at various depths within the abdominal cavity. It is important to avoid the antenna coupling through creeping waves, so Ferrite cores are used on the cable entering the pig and also the insertion point was covered with an electromagnetic insulator. The distance between the transmit and receive antennas were measured by using an electromagnetic tracking system, which can estimate the distance with an accuracy of 0,7 mm. To measure the path loss and coupling characteristics between the transmit and receive antennas, a vector network analyser was employed, whose ports were connected to both antennas with shielded coaxial cables. For avoiding touching with abdominal fluids and the skin of the pig, both transmit and receive antennas were covered with a layer of nitrile butadiene rubber. Let us show the distance dependency of the average path loss characteristics at UWB low-band (from 3,4 GHz to 4,8 GHz) measured in the living animal experiment in Figure 10. Figure 10 shows the path loss characteristics in two cases of excitation at either Port one or two shown in Figure 8 (b). It should be noted that an acceptable level of path loss performance is achieved.

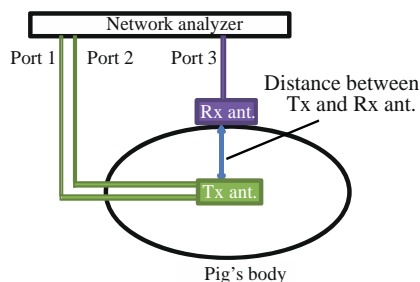


Figure 9: Overview of experimental environment with a living animal

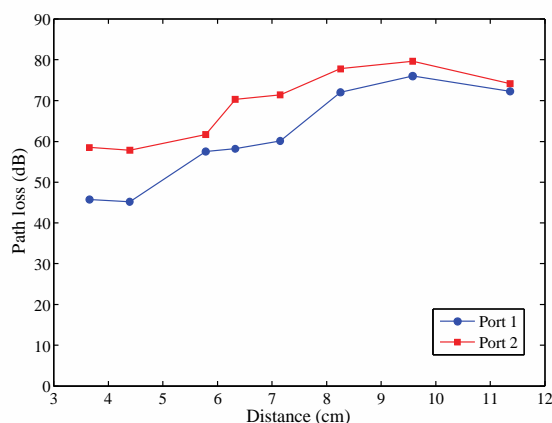


Figure 10: Measured path loss performance in the experiment

8.3 Improvement of communication performance

Then, the improvement of the communication performance by the implant side diversity system was evaluated. In this paper, the communication performance was discussed in a viewpoint of Signal-to-Noise power Ratio (SNR). In order to perform the performance evaluation, not only a case of transmit diversity with the Maximum Ratio Combining (MRC) model but also a case of a single transmit antenna (namely, a case without transmitting diversity) is assumed. In the evaluation, it was assumed that two transmit antennas were alternately used for signal transmission. For investigating the communication performance with the transmit diversity, it is important to take into consideration of a correlation coefficient between the two channels from each transmit antenna to the receive antenna. Here, the correlation coefficient $\rho = 0,51$ is chosen, which was obtained in the measurement at 3,4 GHz to 3,6 GHz UWB low-band. Finally, Table 1 summarizes the simulation parameters.

Table 1: Parameters of communication performance evaluation

Number of trials	1,000,000
Propagation model	Log-normal distribution
Parameter of log-normal distribution	1,80
Correlation coefficient ρ	0, 0,51
Threshold for outage rate	-90 dBm
Transmit diversity scheme	MRC with two branches

The cumulative distribution function (*c.d.f*) on the SNR characteristics at the receiver side is demonstrated in Figure 11. From the results in Figure 11, the transmit diversity with the developed antenna improved the SNR by around 4 dB as compared with the single antenna case when the cumulative probability is 0,8. Furthermore, similar SNR improvement is accomplished in the two cases for the correlated and perfectly uncorrelated cases, which means that the correlation coefficient obtained in the developed transmit antenna is acceptable for the polarization diversity.

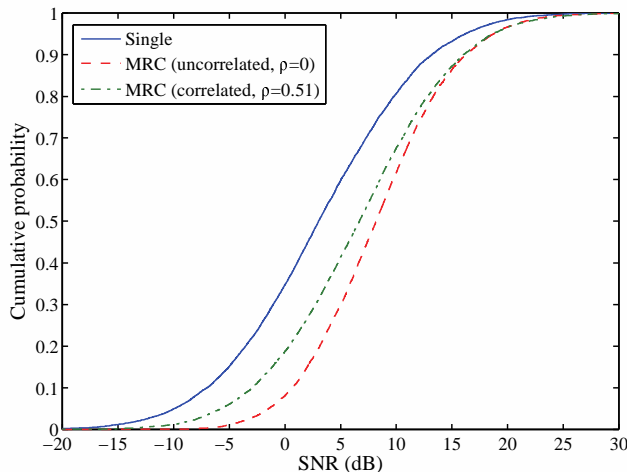


Figure 11: Cumulative distribution function of SNR characteristics

9 Implantable Device Localization with UWB Communications

9.1 Location Estimation System Based on RSSI

In the location estimation system, there is a medical implantable device inside a human body whose location is unknown so should be estimated and N receivers on the body surface whose locations are known in advance. Here, the receivers, namely RSSI detectors, measure RSSI data from UWB implant communication signals transmitted by the implantable device. The system estimates the two-dimensional implantable device location $u = [x, y]^T$ based on N receiver positions $a_n = [x_n, y_n]^T$, where the index n ranges between 1 and N . The implantable device transmits a packet to the receivers, and each receiver measures an RSSI P_n from the received packets. To accurately estimate the implantable device location with RSSI, a statistical model on the RSSI is required, which can well characterize the RSSI variation in the implant communication. From the investigation based on the finite difference time domain analysis, it is concluded that the RSSI of the 400 MHz MICS-band signals can be well modelled with the following two-layered model:

$$p(P_n|r_n) = \frac{1}{\sqrt{2\pi}\sigma P_n} \exp\left[-\frac{\{\log P_n - \log \bar{P}_n\}^2}{2\sigma^2}\right] \quad (1)$$

$$\bar{P}_n = \alpha r_n^{-\beta} \quad (2)$$

where P_n and r_n indicate the average received power and the distance between the implantable device and the n -th receiver, respectively, and $p(P|r)$ is the conditional probability density function (*p.d.f.*) on P_n when r_n is given. From the above equations, the channel parameters vector should be defined as $\mathbf{c} = [\alpha, \beta, \sigma]^T$ that is uniquely determined by individual human body characteristics. To estimate the implant device location, it is needed to derive a log-likelihood function on the implant device location u as $L(u) = \log l(u) = \log p(P_1, P_2, \dots, P_n|u)$. Assuming that P_n is statistically independent with $P_{n'}$ ($n \neq n'$) (*local whiteness*), the following equation is finally obtained:

$$L(u) = \sum_{n=1}^N \left\{ -\log[\sqrt{2\pi}\sigma P_n] - \frac{\{\log P_n - \log \bar{P}_n\}^2}{2\sigma^2} \right\} \quad (3)$$

The ML location estimation gives \hat{u} which maximizes the likelihood function $L(u)$, where $(\hat{\cdot})$ denotes the estimate of (\cdot) .

Then, a prototype hardware system of the ML location estimation with the UWB communications was developed. A transceiver using the UWB communications was developed on a FPGA (Field Programmable Gate Array) board. Figure 12 shows the structure of the transceiver. The receiver was consisted of four RF units to obtain received signals at each antenna simultaneously. In the receiver, a peak hold circuit was inserted before the input to the ADC (Analog-to-Digital Converter), so that, the peak voltage of the UWB pulse can be obtained as a digital value with a sampling rate of only 200 kHz. As for transmitting and receiving antennas, a 1-wavelength loop antenna was employed and unbalanced plane dipole antennas, respectively.

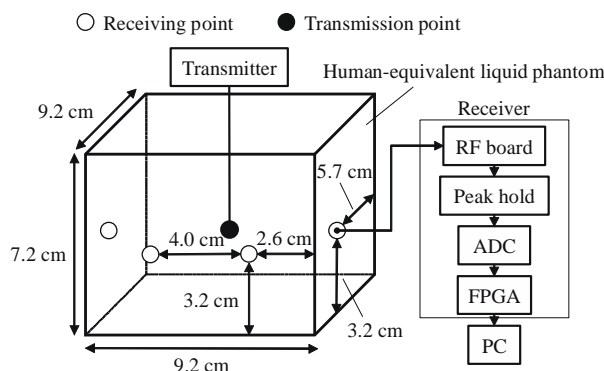


Figure 12: Location estimation system

9.2 Experimental Evaluation on RSSI-Based Localization

In order to evaluate the estimation accuracy, an experiment was performed with a biological equivalent liquid phantom as shown in Figure 13. The transmit antenna was arranged at a total of 10 positions at 10 mm intervals inside the liquid phantom. The location estimation area was the same as the size of the liquid phantom. In addition to the evaluation of the developed UWB location estimation system, a location estimation experiment was carried out for the 400 MHz MICS band-based localization system, which is mainly used in a commercially-available capsule endoscope.

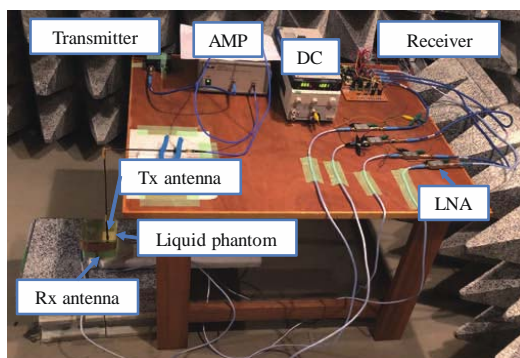


Figure 13: Experimental setup for RSSI-based localization system

Figure 14 shows the cumulative probability distribution of the estimation accuracy for the developed UWB system and the 400 MHz-band system. The experimental results show that the developed UWB system achieves better estimation accuracy than the location estimation systems with the 400 MHz MICS band in the aid of the high distance resolution of the UWB communication signals. Besides, the RMSE (Root Mean Squared Error) of the developed system is achieved to 3,9 mm, on the other hand, the RMSE of the MICS band results in 16,0 mm, which indicates the developed localization system accomplishes 25 % improvement in RMSE characteristics, compared with a typical localization system based on 400 MHz band.

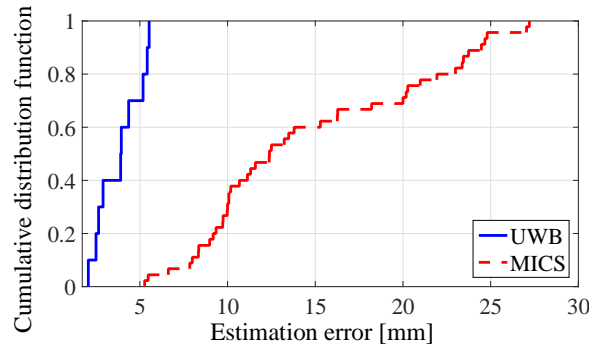


Figure 14: Cumulative distribution function on position estimation error

9.3 Location Estimation System Based on TOA

Here, the Time Of Arrival (TOA)-based location estimation is considered because it can achieve much higher localization accuracy than other RF-based location estimation such as RSSI-based methods. However, whereas the propagation velocity in free space is always constant, the propagation velocity inside a human body should be different from one in free space because wireless signals transmitted from a WCE pass through various kinds of human tissues. Therefore, it is important to estimate the propagation velocity for accurately tracking the WCE location with the TOA technique. The variation of propagation velocity is mainly affected by the relative permittivity of human body tissues, so the propagation velocity can be estimated by using the relative permittivity information. In the related works, for example, in order to obtain the relative permittivity information, images of the inside of a human body are acquired beforehand from a Magnetic Resonance Imaging (MRI) or Computed Tomography (CT) system. For considering the use in reality, troublesome pre-measurement of the human body structure is unsuitable to the WCE systems. Therefore, in the present document, both the WCE location and the relative permittivity are simultaneously estimated, instead of pre-measurement for the relative permittivity information in advance. For this purpose, the relative permittivity estimation model with measured RSSI information is derived.

As for the transmitted wireless signal, an UWB-IR pulse is employed whose frequency band is assumed to 3,4 GHz to 4,8 GHz (UWB low-band). Note that the TOA τ can be detected by using the calculation of the cross-correlation between the transmitted and received signals, and the RSSI E is determined as the peak received electric field intensity of the received UWB-IR pulse. Furthermore, based on the measured TOA τ , under the condition of the usage of high frequency, the transceiver distance can be estimated as

$$\hat{d}(\tau, \varepsilon_r) = \frac{c}{\sqrt{\varepsilon_r}} \tau \quad (4)$$

where c and τ the speed of light and the relative permittivity of a human body, respectively. The above equation means that estimation of the transceiver distance requires both the TOA τ and the relative permittivity ε_r .

For introducing the TOA technique into WCE location estimation, the relative permittivity ε_r should be also required. In the present document, ε_r is estimated based on the RSSI information (RSSI means E as defined below). Because a human body is actually composed of various kinds of biological tissues, several lossy dielectrics exist between the transmitter (WCE) and the receiver. For simplification of the estimation problem, this paper assumes that there is only one biological tissue between the WCE and the receiver, which has the electric constants (namely, the relative permittivity and conductivity) averaged over the several lossy dielectrics. In this case, assuming that the transmitted signal radiates in a spherical waveform, the received electric field intensity, that is, the RSSI E can be approximately expressed as:

$$E = f(\varepsilon_r) = \frac{1}{d} \exp[-\alpha(\varepsilon_r)d] \quad (5)$$

$$\alpha(\varepsilon_r) = \omega \sqrt{\mu_0 \varepsilon_0 \varepsilon_r} \operatorname{Im} \left[\sqrt{1 - j \frac{\sigma}{\omega \varepsilon_0 \varepsilon_r}} \right] \quad (6)$$

where E_0 , μ_0 and ω mean the electric field intensity of the transmitted signal on the body surface, the magnetic permeability in free space, and the angular frequency, respectively. Consequently, the relative permittivity can be estimated as

$$\hat{\varepsilon}_r = f^{-1}(E) \quad (7)$$

where $f^{-1}(\cdot)$ indicates the inverse function of $f(\cdot)$ defined in the above equation.

9.4 Performance Evaluation on TOA-Based Localization

First, let us validate the proposed relative permittivity estimation model. For the validation, Finite Difference Time Domain (FDTD) simulations were employed. The employed anatomically human body model, which was developed by the National Institute of Information and Communication Technology, Japan. The human body model is 1,73 m tall and 65 kg weight and is composed of 51 kinds of biological tissues with a spatial resolution of 2 mm. The transmit antenna of the WCE was assumed inside the small intestine of the human body, and the receive half-wavelength dipole antennas were placed at five locations on the body surface. In the FDTD simulations, a 2-mm long dipole as the transmit antenna was moved to have 15 locations inside the small intestine.

Figure 15 shows the FDTD-simulated results for the validation of the relative permittivity estimation model. From these results, the relationship between the relative permittivity and the received electric field intensity is well expressed by the proposed model because the correlation coefficient between the FDTD-simulated data and the data obtained by the approximated line is 0,702. It is noted that, whereas the proposed relative permittivity estimation assumes only one average biological tissue, a good estimation accuracy of the relative permittivity based on the received electric field intensity is expected to be accomplished.

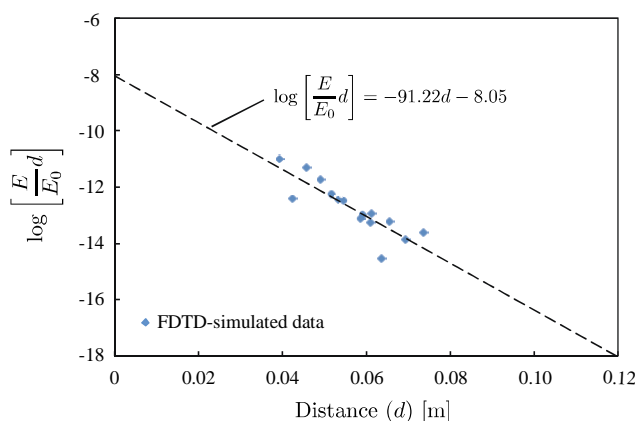


Figure 15: Validation results for relative permittivity estimation model

Next, to evaluate the performances of the proposed joint TOA/RSSI-based location estimation method, computer simulations were performed. In this evaluation, a particle filter to the localization system was applied, which can realize non-linear location tracking. For applying the particle filter algorithm in the implant device localization, it is assumed that the WCE moves inside a small intestine according to a random waypoint model, and the destination location of the transition model was determined based on the small intestine of the anatomical human model in advance. 8 receivers were put at each vertex of the cuboid, which consisted of muscle, fat and skin.

Figure 16 shows the RMS location estimation error for the proposed location estimation method. As can be seen from this figure, as the number of particles increases, the localization performance can be improved at the sacrifice of computational complexity. In all three cases, the localization performance of the proposed tracking method quickly converges to an excellent estimation accuracy. For example, when the number of particles is 10,000, the achievable RMS location estimation error is around 2 mm.

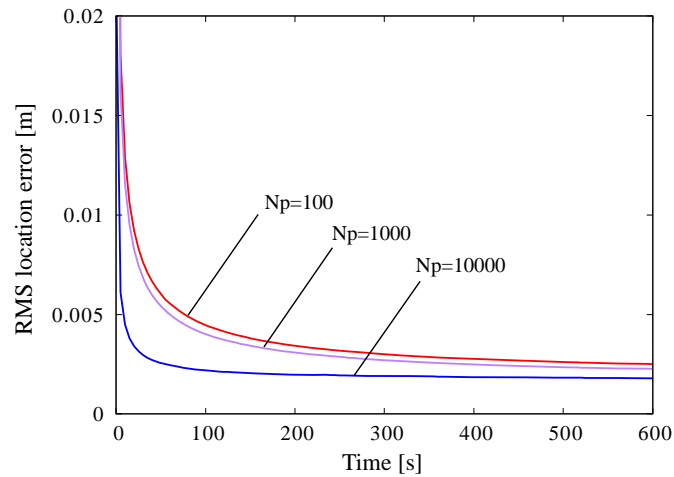


Figure 16: RMSE location estimation error for TOA-based location estimation method

Finally, let us discuss the cumulative distribution function (*c.d.f.*) on the location estimation error for the proposed tracking method. From Figure 17, the maximum location estimation error of the proposed location estimation method is achieved within 4 mm. Furthermore, when the *c.d.f.* of the location estimation error is 0,8, the proposed tracking method can accomplish the accuracy of around 2 mm in the case of the number of particles of 10,000.

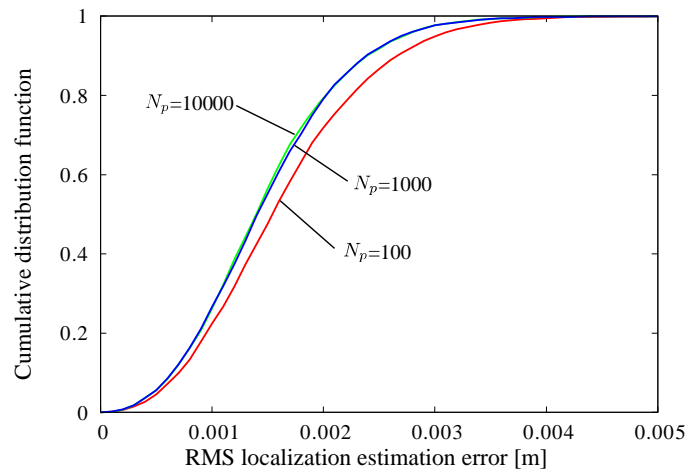


Figure 17: *c.d.f.* of location estimation error for TOA-based localization

History

Document history		
V1.1.1	April 2021	Publication